JOURNAL OF MATERIALS SCIENCE 32 (1997) 2687–2692

Structural evolution during calcination of sol–gel synthesized alumina and alumina–8 vol % zirconia composite

J. KUO, D. L. BOURELL
Center for Materials Science and Engineering, C2201, The University of Texas at Austin, Austin, TX 78712, USA

Alumina and alumina–8 vol % zirconia (3 mol % yttria) composite powders were synthesized via a sol–gel process using metal chlorides as precursors. Sol–gel synthesized alumina and alumina–zirconia composite powders were initially amorphous and contained structural water. Calcination was necessary to drive off the water and prompt crystallization of the powder. Calcination of synthesized powder was performed at various temperatures from 400–1300 °C. Powder morphology and phase evolution during calcination were established using electron microscopy, X-ray diffraction, and thermogravimetric analysis.

1. Introduction

With increasing demand in the quality of advanced ceramics, much research is being devoted to producing nanocrystalline ceramic powder. Nanocrystalline ceramic powder promises high purity with homogeneity at the molecular level and submicrometre grain size after consolidation. Those advantages may eliminate time-consuming milling and mixing steps in conventional ceramic powder preparation, which makes nanocrystalline ceramic powder very attractive for the fabrication of high-quality advanced ceramics. A number of nanocrystalline ceramic powders, such as TiO_2 [1–5], Al_2O_3 [5–12], ZrO_2 [5, 7, 13–20], and SiO_2 [6], have been produced by various methods. The sintering temperature of those nanocrystalline powders is lower than that of conventional powder [7, 9, 11, 15–17, 21–23]. This is attributed to the shorter diffusion length and higher surface curvature of nanosized powder. Both help to lower the sintering temperature and minimize coarsening. Submicrometre final grain size not only makes the consolidated parts stronger [9, 24, 25], but also makes ceramics candidates for superplastic processing [26–30], because fine structure is a prerequisite for superplasticity [31, 32].

Sol–gel synthesis has several advantages over other methods for producing nanocrystalline ceramic powder. Sol–gel synthesis involves minimal capital investment, produces an acceptable amount of output, can be easily scaled up, and can accommodate multicomponent compounds. Winnubst *et al.* [14] synthesized nanocrystalline Y_2O_3-doped ZrO_2 powder with 8 nm crystallite size with two different precursors, metal chlorides and metal alkoxides. They found that the microstructure of the powder synthesized from chlorides was preferable to the powder synthesized from alkoxides, because the former did not aggregate. We previously followed the chloride synthesis route and demonstrated excellent sinterability of the chloride-synthesized Y_2O_3-doped ZrO_2 powder [16]. In the present study, that technique was used again to synthesize alumina and alumina–8 vol % zirconia composite powder. Because the synthesized product was in the form of hydroxides, subsequent calcination was required to drive off the structural water and transform the hydroxides to transition aluminas and, finally, alpha alumina. This paper presents the microstructural development and phase evolution of synthesized powder during calcination at different temperatures.

2. Experimental procedure

The precursor used for making alumina was $AlCl_3 \cdot 6H_2O$. For alumina–8 vol % zirconia (3 mol % yttria), $YCl_3 \cdot 6H_2O$ and $ZrCl_4$ were used as well. The precursors were weighed and dissolved in 0.4 M HCl. While the solution was stirred with a 37 mm propeller, NH_4OH was added until the pH reached 11. The gel was then washed four times with decreasing amounts of ammonia in aqueous solution. Finally, the gel was washed three times with ethanol to remove free water. The gel was dried in air at 120 °C for 16 h. The powder thus obtained was ground using an agate mortar. Calcination of the powder was carried out in air and in batches at temperatures between 400 and 1300 °C for 2 h.

Phases present in the powder at different stages and the crystallite sizes were determined by X-ray diffraction (XRD) using a Philips X-ray diffractometer, Model PW 1729, with CuK_α radiation. The scanning rate was $2^\circ\,min^{-1}$. "JADE" software, developed by Materials Data Inc., was used to analyse the XRD data.

Microstructural evolution of the powder was observed using transmission electron microscopy (TEM,

Jeol 200CX) and scanning electron microscopy (SEM, Jeol JSM-35CX). Powder for TEM observation was dispersed in acetone and dripped on to a 3 mm copper grid covered with holey carbon film. The powder for SEM observation was spread on to a conductive tape and sputtered with a thin layer of a Au–Pd alloy to prevent charging.

Thermogravimetric analysis (TGA) was conducted in bottled air on pure alumina gel immediately after the gel was dried at 120 °C for 16 h. A Perkin–Elmer Series 7 thermal analysis system was used. The temperature range was from 50–1000 °C at a heating rate of 5 °C min^{-1}.

3. Results and discussion

3.1. X-ray diffraction

X-ray diffraction (XRD) patterns of the calcined alumina powder are shown in Fig. 1 as a function of calcination temperature. Powder A-120 (gel dried at 120 °C for 16 h) showed both sharp peaks and broad peaks. The sharp peaks belong to bayerite ($Al(OH)_3$), which is well crystallized. The broad peaks were identified as pseudoboehmite, or poorly crystallized boehmite (γ-AlOOH). Pseudoboehmite is a solid whose XRD pattern shows broad lines that coincide with the major reflections of well-crystallized boehmite [33].

At 400 °C (A-400; A-alumina, AZ-composite, and the drying/calcination temperatures are given), both pseudoboehmite and bayerite were dissociated, all the peaks disappeared and the powder appeared to be amorphous. At 550 °C (A-550), gamma alumina (and/or eta alumina) peaks appeared and remained through 800 °C calcination (A-800). X-ray diffraction could not clearly distinguish between gamma alumina and eta alumina; therefore, gamma is used to denote both phases in the following text. At 900 °C (A-900), gamma alumina peaks disappeared and those corresponding to theta alumina appeared. Theta alumina was the only phase present in A-1000 and A-1100. The final phase, alpha, emerged in A-1200, where it coexisted with theta. Theta alumina disappeared when the powder was calcined at 1300 °C (A-1300), and alpha alumina was the only remaining phase in the powder.

Similar XRD patterns of the alumina–8 vol % zirconia composite powder are shown in Fig. 2. Unlike A-120, AZ-120 showed no crystalline phase at all. Winnubst *et al.* [34] synthesized a ZTA (85 wt % Al_2O_3) powder with a method similar to ours. They observed crystalline bayerite in their 120 °C-dried ZTA powder; however, no crystalline bayerite was observed in our powder.

In AZ-400, no crystalline phase was observed. In both AZ-550 and AZ-800, gamma alumina was present. In AZ-900 and AZ-1000, peaks corresponding to theta alumina and tetragonal zirconia appeared, while those from gamma alumina still remained. The gamma phase finally disappeared in the powder calcined at 1100 °C. In AZ-1200, theta alumina and tetragonal zirconia were the only phases present. In AZ-1300, alpha alumina replaced theta alumina and coexisted with tetragonal zirconia. The disappearance of gamma alumina and the appearance of theta alumina occurred at a higher temperature in the composite powder than in pure alumina. In our previous study [16], yttria-stabilized tetragonal zirconia was well crystallized when calcined at 550 °C, but in the current study, crystallization did not start until 900 °C and sharp peaks were not obtained until 1300 °C. Apparently, the coexistence of alumina and zirconia inhibits crystallization of both. The implication that alumina and zirconia were intimately mixed was later confirmed by microstructural analysis of our sample.

A summary of the phases present in the powders after calcination is given in Table I. Generally, boehmite and bayerite undergo different transformation routes to the final phase, alpha alumina [33]. These routes are:

$$\text{boehmite} \rightarrow \text{gamma} \rightarrow \text{delta} \rightarrow \text{theta} \rightarrow \text{alpha}$$

(delta alumina does not appear in the decomposition sequence of pseudoboehmite [35]), and

$$\text{bayerite} \rightarrow \text{eta} \rightarrow \text{theta} \rightarrow \text{alpha}$$

According to Table I, the powder generally followed those transformation routes. The structure of gamma, eta, delta, and theta are all deformed spinels with aluminium cations occupying either tetrahedral or octahedral sites in an oxygen anion sublattice. Alpha alumina (corundum) consists of aluminium cations occupying octahedral sites in a hexagonally close-packed oxygen sublattice. Therefore, the transformations

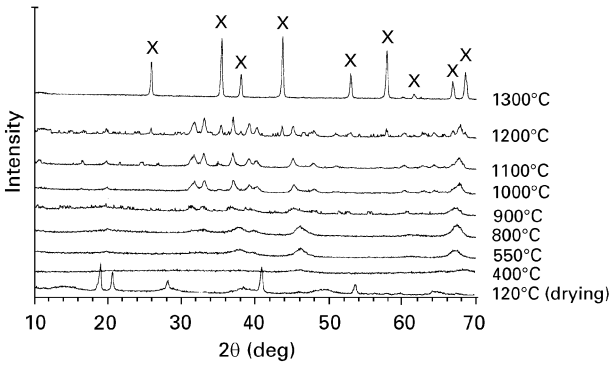

Figure 1 Phase evolution of pure alumina powder with increasing calcination temperature; powder was calcined for 2 h in air after drying for 16 h at 120 °C. (×) Alpha alumina.

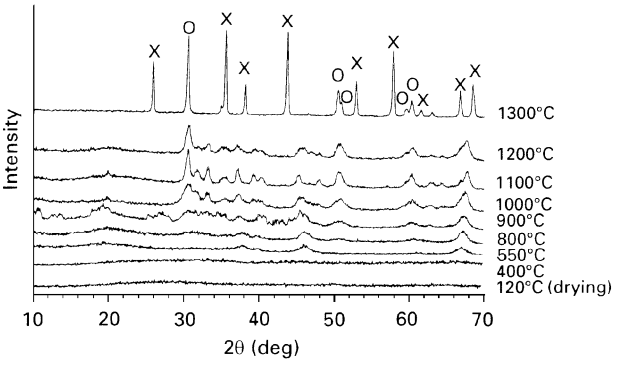

Figure 2 Phase evolution of alumina–8 vol % zirconia powder with increasing calcination temperature; powder was calcined for 2 h in air after drying for 16 h at 120 °C. (×) Alpha alumina, (○) tetragonal zirconia.

TABLE I Phases present and crystalllite size in the alumina and alumina–8 vol % zirconia powder after calcination at various temperatures

	Alumina		Alumina–zirconia composite			
			Alumina		Zirconia	
T (°C)	Phase[a]	Size (nm)	Phase[a]	Size (nm)	Phase[a]	Size (nm)
120 (drying)	Ba + P	–	–	–	–	–
450	–	–	–	–	–	–
550	[b]	5	[b]	4	–	–
800	[b]	5	[b]	6	–	–
900	θ	13	θ,[b]	6	T	6
1000	θ	14	θ,[b]	13	T	8
1100	θ	16	θ	20	T	17
1200	θ, α	27	θ	32	T	21
1300	α	35	α	47	T	33

[a] Ba, Bayerite; P, Pseudoboehmite; θ, theta alumina; α, alpha alumina; T, tetragonal zirconia; –, amorphous state/size not available.
[b] γ and/or η alumina.

among transition aluminas are of the reordering type, while the transformation between theta alumina and alpha alumina is of the massive type.

In the present study, the crystallite size calculated from X-ray peak broadening remained almost unchanged after calcination below 800 °C. As the calcination temperature was increased above 800 °C, crystallites coarsened, and they did so dramatically above 1300 °C. Wefers and Misra [33] reported significant sintering and three-dimensional fusion of transition alumina above 827 °C. Their explanation for enhanced sintering and increased cation mobility in association with conversion to α-alumina, is corroborated by our observation of particle coarsening.

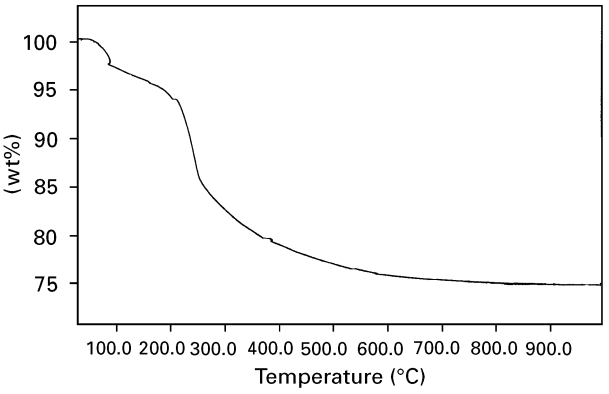

Figure 3 TGA result for alumina powder after drying for 16 h at 120 °C. The initial powder weight was 46.486 g.

3.2. Thermal analysis

The TGA result for the alumina powder is shown in Fig. 3. The sample weight decreased abruptly between 210 and 250 °C, and weight loss continued up to 900 °C. The total weight loss after heating to 1000 °C was 25%. XRD analysis showed pseudoboehmite and bayerite were the two phases present in the 120 °C treated powder. The weight loss of boehmite and bayerite, upon dehydration, was 15% and 35%, respectively [36]. Therefore, the weight percentage of pseudoboehmite and bayerite in the dried powder might be estimated to be approximately 50% of each. Pseudoboehmite converts to crystalline bayerite, the phase thermodynamically stable in air, when aged in an aqueous solution at temperatures under 77 °C [33]. In our case, it is not known whether both bayerite and pseudoboehmite were the hydroxides that formed during synthesis, or whether pseudoboehmite was first formed and then partially converted to bayerite.

3.3. Electron microscopy observation

Microstructures of the pure, calcined nanocrystalline alumina powders, A-120, A-550, A-900, A-1100, and A-1300, were observed using TEM and are shown in Fig. 4a–e respectively. The microstructure of A-120 (Fig. 4a) consists of two distinctively different features. One is faceted particles of nominal size 250 nm (central region of Fig. 4a). Those particles have a mottled appearance which is consistent with a pore network described by Wefers and Misera [33]. Such porosity is associated with the decomposition of aluminium hydroxides during calcination. The pores are described in transition alumina as an intersecting pore system with 1 nm size parallel pores located in the cleavage plane (0 0 1). The parallel pores separate the solid into lamellae that are of the order of 2–3 nm thick, while a network of irregularly shaped slits extends perpendicular to the pores parallel to (0 0 1). The result is an intersecting pore system that divides the lamellae into interconnected, irregularly shaped domains of solid.

The selected-area diffraction (SAD) pattern yielded spots indicating the existence of a crystalline structure. This spot pattern was indexed as eta alumina. However, when a micro-electron beam was used to examine the powder, the diffraction pattern obtained was that of bayerite single crystals, as shown in the insert of Fig. 4a, and not of eta alumina. Because eta alumina is the first transition alumina into which bayerite transforms when it is heated, we believe the heat generated by electron-beam bombardment is responsible for the transformation from bayerite to eta alumina. Also apparent in Fig. 4a is an agglomerated cluster of particles approximately 4 nm in size. The diffraction pattern from this region consisted only of

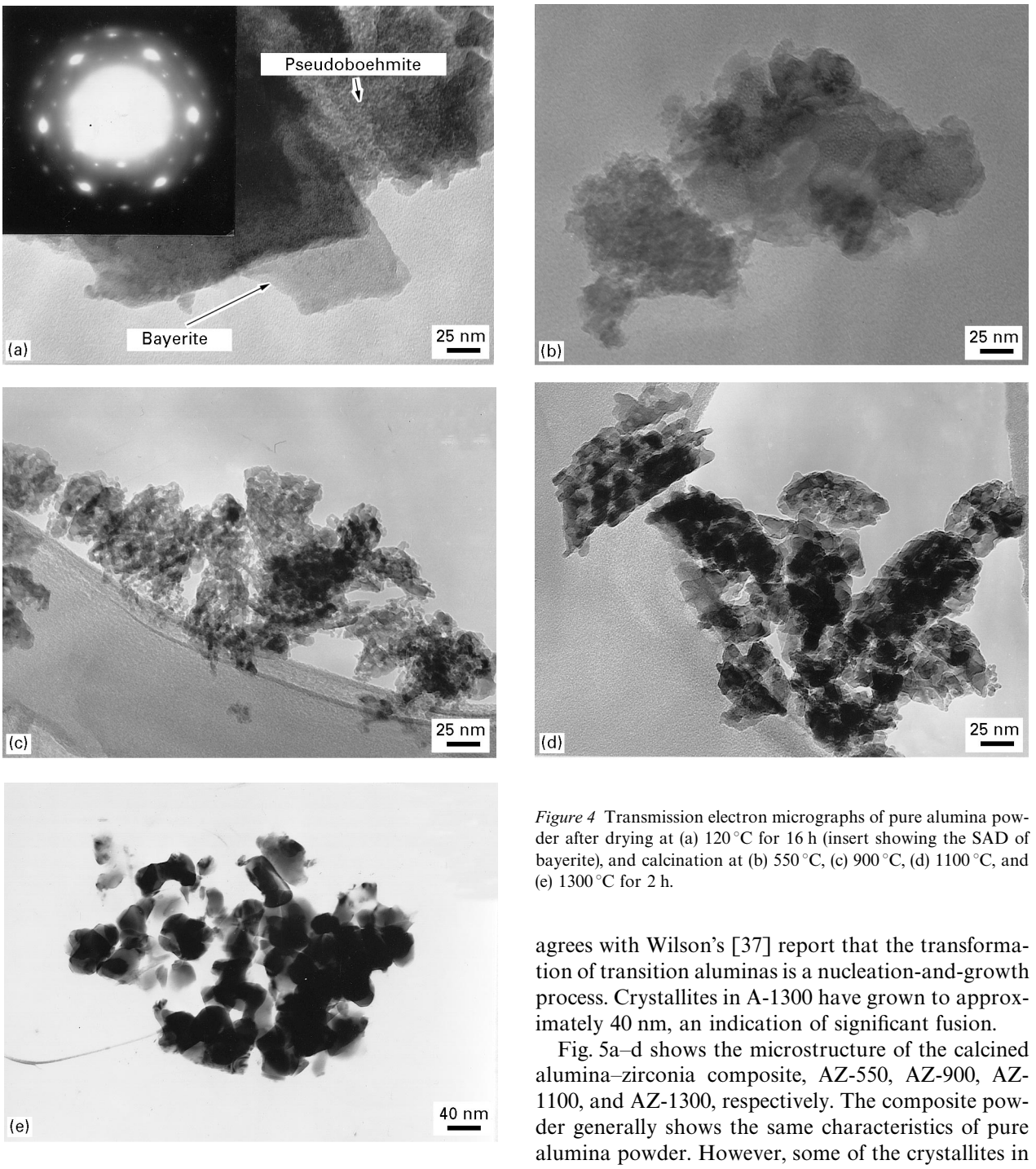

Figure 4 Transmission electron micrographs of pure alumina powder after drying at (a) 120 °C for 16 h (insert showing the SAD of bayerite), and calcination at (b) 550 °C, (c) 900 °C, (d) 1100 °C, and (e) 1300 °C for 2 h.

faint rings, consistent with a nanocrystalline assemblage. We believe that this cluster is the pseudoboehmite phase whose presence was indicated by XRD.

Fig. 4b shows the microstructure of A-550. Traces of Moiré fringes can barely be seen in pseudoboehmite. The pores in bayerite have slightly enlarged. No other changes were observed in A-550. Fig. 4c, d and e show the microstructure of A-900, A-1100, and A-1300, respectively. The pores observed in hydroxides enlarged progressively with increasing calcination temperature. Individual crystallites are visible in Fig. 4c–e, although they have retained the "interconnected" feature from the hydroxides and are heavily aggregated. In A-900, typical crystallite size is 15 nm but with some variation, and the aggregate size is about 100 nm. The inhomogeneity of crystallite size agrees with Wilson's [37] report that the transformation of transition aluminas is a nucleation-and-growth process. Crystallites in A-1300 have grown to approximately 40 nm, an indication of significant fusion.

Fig. 5a–d shows the microstructure of the calcined alumina–zirconia composite, AZ-550, AZ-900, AZ-1100, and AZ-1300, respectively. The composite powder generally shows the same characteristics of pure alumina powder. However, some of the crystallites in AZ-900, AZ-1100, and AZ-1300 appear darker than pure alumina powder. The darker crystallites are most likely zirconia, because zirconia would appear darker due to mass contrast. The zirconia crystallites, as shown in AZ-1300, are smaller than the alumina crystallites. This result agrees with the size measured from X-ray peak broadening. Our earlier hypothesis that zirconia crystallites form an intimate mixture with alumina crystallite is also confirmed by AZ-1300.

Fig. 6 is a scanning electron micrograph of AZ-550. Almost all the powder is agglomerated to various sizes from less than 1 μm to more than 10 μm. No unagglomerated powder was observed in the micrograph. Aggregates or agglomerates can be disadvantageous if they are difficult to break up during compaction of the powder. The large voids between the agglomerates will prolong the sintering time and the final grain size

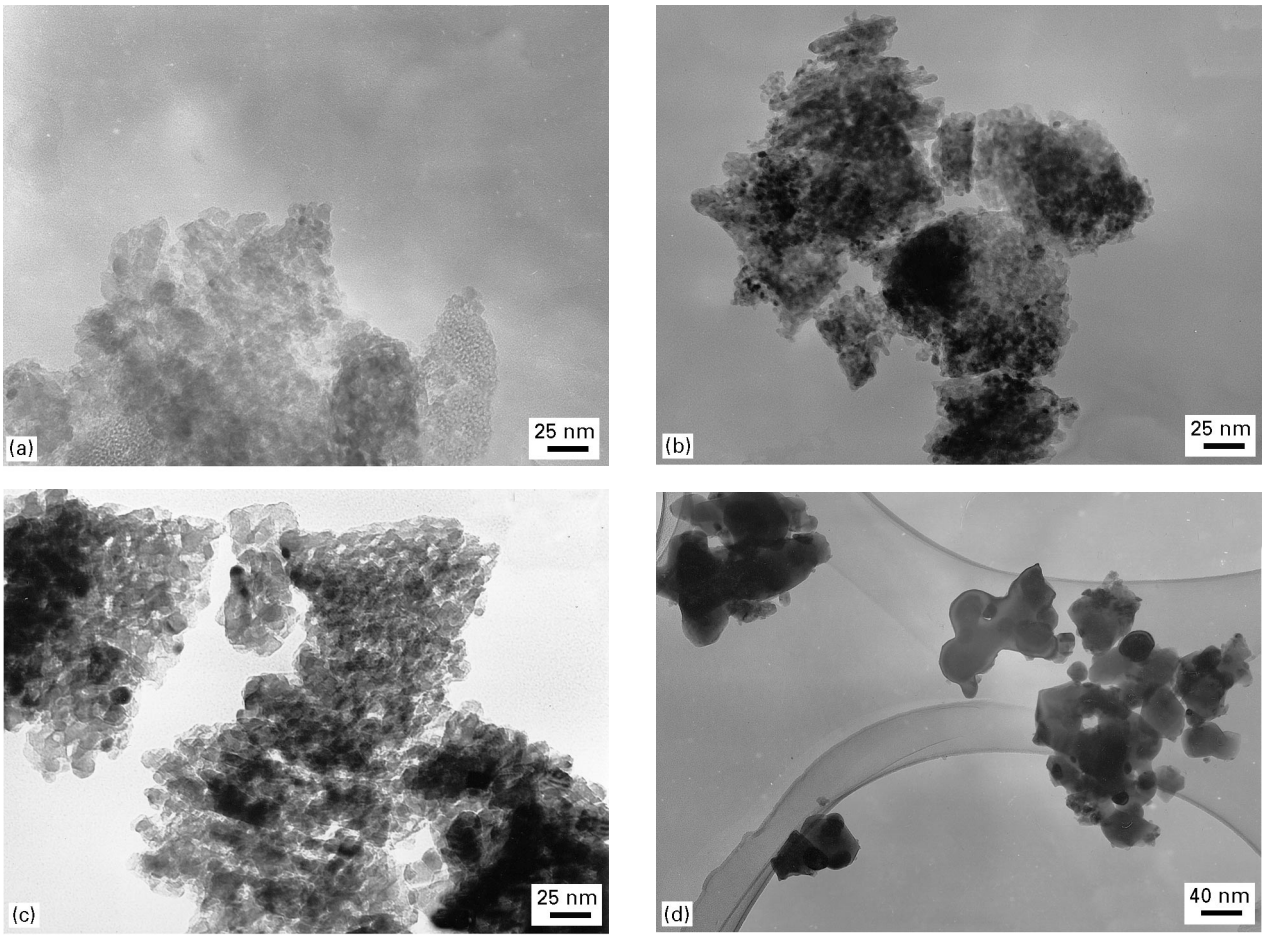

Figure 5 Transmission electron micrographs of alumina–8 vol % zirconia powder after calcination for 2 h at (a) 550 °C, (b) 900 °C, (c) 1100 °C, and (d) 1300 °C.

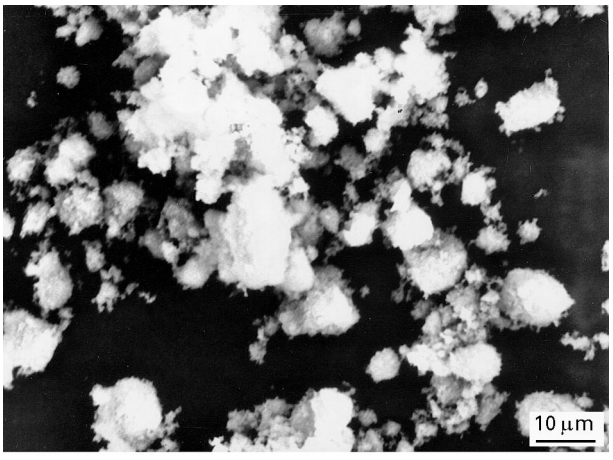

Figure 6 Scanning electron micrograph of alumina–8 vol % zirconia powder after calcination at 550 °C for 2 h, showing the variation of agglomerate size.

will be larger than that of unagglomerated powder. The major benefit of nanosized powder is thus lost.

4. Conclusion

Al_2O_3 and Al_2O_3–8 vol % ZrO_2 were synthesized via a sol–gel method. Bayerite crystals and pseudoboehmite were produced. The proportion of each hydroxide in the powder was estimated from weight loss analysis to be approximately 50% each. The hydroxides were calcined at different temperatures from 400–1300 °C. With increasing calcination temperature, the hydroxides dehydrated and transformed to transition alumina, eventually reaching a final phase alpha alumina. In the composite powder, tetragonal zirconia was the final phase. The coexistence of zirconia and alumina in the composite did not affect the transformation route of the hydroxides. However, the temperature at which the transformation was completed was affected by the presence of zirconia. Similarly, the crystallization of zirconia in alumina was delayed to 900 °C, rather than 550 °C where it has previously been observed to crystallize.

TEM observation of the powder showed that agglomerated clusters of pseudoboehmite and bayerite single crystals both are porous. Pore size increased as the calcination temperature increased. The crystallite size also increased with calcination temperature, although the precise crystallite size may not be assessed directly from transmission electron micrographs due to particle clustering. The crystallite size increased dramatically after conversion to alpha alumina was complete.

Sol–gel synthesized zirconia particles using metal chlorides as the precursors, are spherical, and each particle is discrete [14, 16]. However, our alumina and alumina–zirconia composite powders had an irregular shape and formed aggregates, although the crystallite size was still within the nanometre range.

References

1. H. HAHN, J. LOGAS and R. S. AVERBACK, *J. Mater. Res.* **5** (1990) 609.
2. J. A. EASTMAN, *J. Appl. Phys.* **75** (1994) 770.
3. E. HARO-PONIATOWSKI, R. RODRIGUEZ-TALAVERA, M. DELA CRUZ HEREDIA, O. CANO-CORONA and R. ARROYO-MURILLO, *J. Mater. Res.* **9** (1994) 2102.
4. F. W. YAN and W. W. RHODES, *Mater. Sci. Eng.* **61** (1983) 59.
5. D. VOLLATH and K. E. SICKAFUS, *J. Nanostr. Mater.* **1** (1992) 427.
6. B. GÜNTHER and A. KUMPMANN, *ibid.* **1** (1992) 27.
7. R. CHAIM, *ibid.* **1** (1992) 479.
8. J. A. EASTMAN, L. J. THOMPSON and D. J. MARSHALL, *ibid.* **2** (1993) 377.
9. S. RAJENDRAN, *J. Mater. Sci.* **29** (1994) 5664.
10. Y. MIZUSHIMA and M. HORI, *J. Non-Cryst. Solids* **167** (1994) 1.
11. G. P. JOHNSTON, R. MUENCHAUSEN, D. M. SMITH, W. FAHRENHOLTZ and S. FOLTYN, *J. Am. Ceram. Soc.* **75** (1992) 3293.
12. S. RAJENDRAN and J. L. WOOLFREY, *Key Eng. Mater.* **53–55** (1991) 462.
13. T. OKUBO and H. NAGAMOTO, *J. Mater. Sci.* **30** (1995) 749.
14. A. J. A. WINNUBST, W. F. M. GROOT ZEVERT, G. S. A. M. THEUNISSEN and A. J. BURGGRAAF, *Mater. Sci. Eng.* **A109** (1989) 215.
15. D. L. BOURELL, PARIMAL and W. KAYSSER, *J. Am. Ceram. Soc.* **76** (1993) 705.
16. G. B. PRABHU and D. L. BOURELL, *J. Nanostr. Mater.* **6** (Nano '94 Proceedings, Part I) (1995) 361.
17. PARIMAL, Master Thesis, University of Texas at Austin (1992).
18. K. R. VENKATACHARI, D. HUNG, S. P. OSTRANDER, W. A. SCHULZE and G. C. STANGLE, *J. Mater. Res.* **10** (1995) 748.
19. K. R. VENKATACHARI, D. HUNG, S. P. OSTRANDER, W. A. SCHULZE and G. C. STANGLE, *ibid.* **10** (1995) 756.
20. D. HUANG, K. R. VENKATACHARI and G. C. STANGLE, *ibid.* **10** (1995) 762.
21. M. M. R. BOUTZ, L. WINNUBST, A. J. BURGGRAAF, M. NAUER and C. CARRY, *J. Am. Ceram. Soc.* **78** (1995) 121.
22. M. KUMAGAI and G. L. MESSING, *ibid.* **67** (1984) C-230.
23. Y. J. HE, A. J. A. WINNUBST, H. VERWEIJ and A. J. BURGGRAAF, *J. Mater. Sci.* **29** (1994) 6505.
24. H. HAHN and R. S. AVERBACK, *J. Nanostr. Mater.* **1** (1992) 95.
25. M. YOSHINAKA, K. HIROTA, O. YAMAGUCHI, H. KUME, S. INAMURA, H. MIYAMOTO, N. SHIOKAWA and R. SHIKATA, *Br. Ceram. Trans.* **93** (1994) 234.
26. K. R. VENKATACHARI and R. RAJ, *J. Am. Ceram. Soc.* **69** (1986) 135.
27. T. G. NIEH and J. WADSWORTH, *Acta Metall. Mater.* **39** (1991) 3037.
28. D. M. OWEN and A. H. CHOKSHI, *J. Nanostr. Mater.* **2** (1993) 181.
29. I-WEI CHEN and L. A. XUE, *J. Am. Ceram. Soc.* **73** (1990) 2585.
30. K. KAJIHARA, Y. YOSHIZAWA and T. SAKUMA, *Acta Metall. Mater.* **43** (1995) 1235.
31. Y. MAEHARA and T. G. LANGDON, *J. Mater. Sci.* **25** (1990) 2275.
32. T. G. LANGDON, *JOM* **42** (1990) 8.
33. K. WEFERS and C. MISERA, "Oxides and Hydroxides of Aluminum", ALCOA Technical Paper No. 19, Revised (Aluminum Company of America, ALCOA Center, PA, 1987).
34. P. D. EXTER, L. WINNUBST, T. H. P. LEUWERINK and A. J. BURGGRAAF, *J. Am. Ceram. Soc.* **77** (1994) 2376.
35. B. C. LIPPENS and J. J. STEGGERDA, in "Physical and Chemical Aspects of Adsorbents and Catalysts", edited by B. G. Linsen (Academic Press, London, 1970) pp. 171–209.
36. B. E. YOLDAS, *J. Appl. Chem. Biotechnol.* **23** (1973) 803.
37. S. J. WILSON and J. D. C. McCONNELL, *J. Solid State Chem.* **34** (1980) 315.

Received 19 January
and accepted 17 September 1996